AAS 14-251

SEMI-ANALYTICAL GUIDANCE ALGORITHM FOR AUTONOMOUS CLOSE APPROACH TO NON-COOPERATIVE LOW-GRAVITY TARGETS

Paolo Lunghi[*], Michèle Lavagna[†], and Roberto Armellin[‡]

An adaptive guidance algorithm for close approach to and precision landing on uncooperative low-gravity objects (e.g. asteroids) is proposed. The trajectory, updated by means of a minimum fuel optimal control problem solving, is expressed in a polynomial form of minimum order to satisfy a set of boundary constraints from initial and final states and attitude requirements. Optimal guidance computation, achieved with a simple two-stage compass search, is reduced to the determination of three parameters, time-of-flight, initial thrust magnitude and initial thrust angle, according to additional constraints due to actual spacecraft architecture. A NEA landing mission case is analyzed.

INTRODUCTION

Onboard autonomy is a key feature for the next space systems generation. The capability to actively analyze in-loco the operative environment, to select the more scientifically relevant places to explore, and to adapt the system's behavior to detected conditions, increases both the robustness and the flexibility of the vehicle operations, avoiding limitations due to interplanetary distances.

A typical high-autonomy scenario is the close approach to a non-cooperative low-gravity object (e.g. a NEO or an asteroid), finalized to either touch and go operations or landing. In recent years a renewed interest in small celestial bodies populating the Solar System has brought to several studies and mission proposals. The ESA Rosetta probe, launched in March 2004 and awakened from deep space hibernation mode, is expected to perform a rendezvous with the comet 67P/Churyumov-Gerasimenko on May 2014. The release of the lander Philae, with the objective to collect and on-board analyze samples of comet's soil, is planned for the following November. The OSIRIS-REx spacecraft, planned by NASA for launch in 2017, will travel to the near-Earth asteroid (NEA) Bennu, study it in detail, and bring back a sample to Earth. MarcoPolo-R, a project with similar objectives, has been selected by European Space Agency as M-class candidate mission for the launch in 2022. Recently, in the FY2014 budget proposal, NASA has included a plan to robotically capture a small NEA and redirect it safely to a stable orbit in the Earth-moon system where astronauts can visit and explore it.

[*]Ph.D. Candidate, Aerospace Science and Technology Department, Politecnico di Milano, via La Masa 34, 20156 Milano, Italy.

[†]Associate Professor, Aerospace Science and Technology Department, Politecnico di Milano, via La Masa 34, 20156 Milano, Italy.

[‡]Post Doc. Research Fellow, Aerospace Science and Technology Department, Politecnico di Milano, via La Masa 34, 20156 Milano, Italy.

One of the big challenges to deal with, in such a scenario, is represented by the telecommunications delay because of the interplanetary distances, and the necessity to in-loco analyze landing sites and possible trajectories, due to the impossibility to perform a full characterization of the target from the ground: they clearly ask for a high level of onboard autonomy in the Guidance Navigation and Control, coupled with light and fast computational mechanisms.

Different approaches at the landing problem have been adopted during the years. A trajectory based on a quartic polynomial in time was used during the Apollo missions.[1] A derivative of the Apollo lunar descent guidance was still considered in recent years, for the Mars Science Laboratory (MSL).[2] Various other approaches to obtain both numerical and approximate solutions of the pinpoint landing terminal guidance problem have been described over the last few years. Direct numerical methods for trajectory optimization have been widely investigated, not requiring the explicit consideration of the necessary conditions.[3] These methods have been used together with Chebyshev pseudospectral techniques, in order to reduce the number of the optimization variables.[4] Also convex programming approach has been proposed, in order to guarantee the convergence of the optimization.[5] Direct collocation methods has showed that the size of the region of feasible initial states, for which there exist feasible trajectories, can be increased drastically (more than twice) compared to the traditional polynomial-based guidance approaches, but at the price of a higher computational cost.[5]

In the case of asteroids and comets, landing and close proximity operations present some peculiarities, due to their small size and irregular shape. In particular, the gravitational acceleration is very weak and variable in function of the relative position of the spacecraft respect to the target. Due to that, orbits are generally complex and non periodic, and stable only in certain regions.[6] Zero Emission Effort/Zero Emission Velocity guidance had been proved to produce a good approximation of the fuel-optimal trajectory in close proximity maneuvers around asteroids,[7] and it has been applied together with high-order sliding mode control in order to increase robustness to disturbances and unmodeled dynamics.[8,9]

Recently, a semi-analytical approach has been proposed for planetary landing maneuvers, in order to conjugate the low computational cost of polynomial approximation to the larger flexibility of direct optimization methods.[10] This approach has proved effective in reaching a good approximation of the optimum control profile with a low computational cost. In this paper the application of this approach in a low-gravity environment (characterized by long times of flight and low thrust) is investigated.

OPTIMAL GUIDANCE PROBLEM STATEMENT

Dynamical Model

The motion of the spacecraft is modeled in an asteroid-fixed Cartesian frame, centered on the center of mass of the asteroid. Assuming the asteroid rotational rate as constant, the dynamics are described by the well known equations of motion for uniform rotating frames:

$$\dot{\mathbf{r}} = \mathbf{v}, \tag{1}$$

$$\mathbf{a} = \dot{\mathbf{v}} + 2\boldsymbol{\omega} \times \mathbf{v} + \boldsymbol{\omega} \times \boldsymbol{\omega} \times \mathbf{r}, \tag{2}$$

where $\mathbf{r} = [x, y, z]^T$ is the spacecraft position vector, $\mathbf{v} = [v_x, v_y, v_z]^T$ is the velocity vector, $\mathbf{a} = [a_x, a_y, a_z]^T$ is the acceleration vector and $\boldsymbol{\omega}$ is the asteroid rotational rate vector. A two-body model is considered; the spacecraft mass is assumed to be negligible compared to the asteroid. The adopted reference frame is represented in Figure 1.

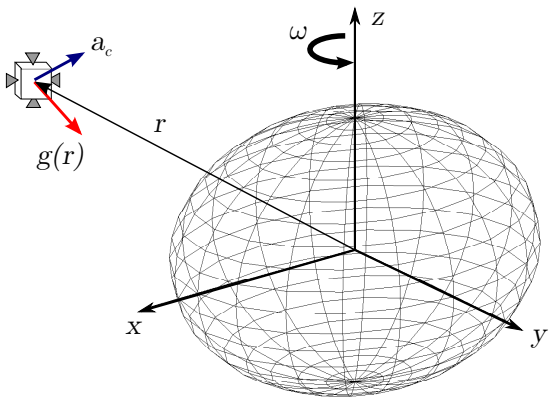

Figure 1. Body-fixed asteroid reference frame.

The acceleration vector acting on the spacecraft consists of different contributions:

$$\mathbf{a} = \mathbf{g}(\mathbf{r}) + \mathbf{a}_\mathrm{c} + \mathbf{d}, \tag{3}$$

$\mathbf{g}(\mathbf{r})$ is the gravitational acceleration, function of the position in the asteroid reference frame, $\mathbf{a}_\mathrm{c} = [a_\mathrm{cx}, a_\mathrm{cy}, a_\mathrm{cz}]^T$ is the control acceleration and $\mathbf{d} = [d_x, d_y, d_z]^T$ is a term that includes disturbances (such as solar pressure or additional gravity terms due to non uniform density or irregular shape).

It is assumed that the asteroid can be modeled as a tri-axial ellipsoid with uniform density ρ. In this way, it is possible to analytically evaluate the gravitational component of the acceleration as the gradient of its potential field $V_g(\mathbf{r})$:[11]

$$\mathbf{g}(\mathbf{r}) = -\nabla\big(V_g(\mathbf{r})\big). \tag{4}$$

Considering the asteroid's rotational rate vector aligned with the z axis, results $\boldsymbol{\omega} = [0, 0, \omega]^T$. Then, the dynamical system can be written in its scalar form as:

$$\dot{x} = v_x, \tag{5}$$

$$\dot{y} = v_y, \tag{6}$$

$$\dot{z} = v_z, \tag{7}$$

$$\dot{v}_x = 2\omega v_y + \omega^2 x - \frac{\partial V_g}{\partial x} + a_\mathrm{cx} + d_x, \tag{8}$$

$$\dot{v}_y = -2\omega v_x + \omega^2 y - \frac{\partial V_g}{\partial y} + a_\mathrm{cy} + d_y, \tag{9}$$

$$\dot{v}_z = -\frac{\partial V_g}{\partial z} + a_\mathrm{cz} + d_z. \tag{10}$$

This system is completed by an additional equation describing the dynamics of the spacecraft mass m, described by:

$$\dot{m} = -\frac{T}{I_\mathrm{sp} g_0}, \tag{11}$$

where T is the norm of the thrust vector $\mathbf{T} = [T_x, T_y, T_z]^T$, I_{sp} is the thrusters specific impulse and g_0 is the standard gravity acceleration at the sea level. The mass equation is linked to the control acceleration that corresponds to the thrust-to-mass ratio:

$$\mathbf{a}_{\text{c}} = \mathbf{T}/m. \tag{12}$$

Then, the equation (11) can be rewritten as:

$$\dot{m} = -\frac{\|\mathbf{a}_{\text{c}}\|}{I_{\text{sp}} g_0} m. \tag{13}$$

which is a first order linear ordinary differential equation whose solution is:

$$m(t) = m_0 \exp\left(- \int_{t_0}^{t} \frac{a_c(t)}{I_{\text{sp}} g_0} dt \right). \tag{14}$$

The analytical calculation of the integral exponent is not simple, but it can be easily obtained trough numerical integration, using pseudospectral methods, such as the Clenshaw-Curtis quadrature.[12]

Trajectory Formulation

At the time instant t_0 in which the landing maneuver is commanded, position $\mathbf{r}_0$ and speed $\mathbf{v}_0$ of the spacecraft are known. On the other hand, At the end of the maneuver, at final time t_{f}, target position $\mathbf{r}_{\text{f}}$ and speed $\mathbf{v}_{\text{f}}$ are required.

From Equations (2) and (3), the initial derivative of the speed depends on the initial control acceleration, which is determined by the initial thrust vector $\mathbf{T}_0$ (disturbances are not taken into account in the guidance algorithm).

During the optimization process, the number n_{eval} of function evaluations for each iteration is $n_{\text{eval}} = \text{O}(2^{n_{\text{var}}})$, where n_{var} is the number of optimization variables. In order to reduce this number, and consequently the computation time of the algorithm, is possible to force the initial thrust vector to lie in the plane defined by vectors $\mathbf{r}_0$ and $\mathbf{r}_f$ (as shown in Figure 2).

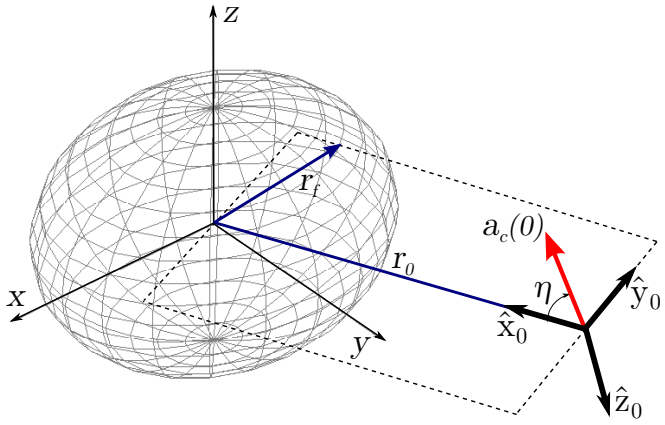

Figure 2. Initial control acceleration.

In order to do that, it is possible to define a local reference frame, aligned with the spacecraft-asteroid direction, whose xy plane contains $\mathbf{r}_0$ and $\mathbf{r}_\mathrm{f}$, through the director cosine matrix:

$$\mathrm{A}_0 = [\hat{\mathbf{x}}_0 \quad \hat{\mathbf{y}}_0 \quad \hat{\mathbf{z}}_0]^T, \tag{15}$$

where:

$$\hat{\mathbf{x}}_0 = -\frac{\mathbf{r}_0}{\|\mathbf{r}_0\|}, \tag{16}$$

$$\hat{\mathbf{z}}_0 = \frac{\mathbf{r}_\mathrm{f} \times \mathbf{r}_0}{\|\mathbf{r}_\mathrm{f} \times \mathbf{r}_0\|}, \tag{17}$$

$$\hat{\mathbf{y}}_0 = \hat{\mathbf{z}}_0 \times \hat{\mathbf{x}}_0. \tag{18}$$

Then, by defining a second matrix, describing a rotation η_0 around $\hat{\mathbf{z}}_0$:

$$\mathrm{A}_\eta = \begin{bmatrix} \cos\eta_0 & \sin\eta_0 & 0 \\ -\sin\eta_0 & \cos\eta_0 & 0 \\ 0 & 0 & 1 \end{bmatrix}, \tag{19}$$

the initial thrust vector $\mathbf{T}_0$ can be obtained, function of the initial thrust magnitude T_0 and of the initial angle of thrust η_0:

$$\mathbf{T}_0 = \mathrm{A}_0^T \mathrm{A}_\eta^T \begin{bmatrix} T_0 & 0 & 0 \end{bmatrix}^T. \tag{20}$$

Then, a total of 15 boundary constraints are available: 6 from initial states, 3 from initial control acceleration and 6 from the desired final states.

$$\mathbf{r}(t_0) = \mathbf{r}_0, \tag{21}$$
$$\mathbf{v}(t_0) = \mathbf{v}_0, \tag{22}$$
$$\dot{\mathbf{v}}(t_0) = \mathbf{f}(T_0, \eta), \tag{23}$$
$$\mathbf{r}(t_\mathrm{f}) = \mathbf{r}_\mathrm{f}, \tag{24}$$
$$\mathbf{v}(t_\mathrm{f}) = \mathbf{v}_\mathrm{f}. \tag{25}$$

Then, the trajectory can be expressed in a polynomial form. The minimum order needed to satisfy boundary constraints is 5:

$$\mathbf{r}(t) = \mathbf{c}_0 + \mathbf{c}_1 t + \mathbf{c}_2 t^2 + \mathbf{c}_3 t^3 + \mathbf{c}_4 t^4 + \mathbf{c}_5 t^5. \tag{26}$$

If $t_0 = 0$:

$$\mathbf{r}(t) = \mathbf{r}_0 + \mathbf{v}_0 t + \frac{\dot{\mathbf{v}}_0}{2} t^2 + \mathbf{c}_3 t^3 + \mathbf{c}_4 t^4 + \mathbf{c}_5 t^5. \tag{27}$$

By deriving Equation (26) as needed and solving for the boundary constraints, a fully defined trajectory can be determined, depending on 3 parameters: time-of-flight $t_\mathrm{tof} = t_\mathrm{f} - t_0$, initial thrust magnitude T_0 and initial angle of thrust η_0. By solving Equations (8), (9) and (10) for $\mathbf{a}_c$ a complete control acceleration profile can be obtained.

Additional Constraints

The problem is reduced to find the values of T_0, η_0 and t_{tof}, according to any additional constraint not implicitly satisfied by the polynomial formulation, in order to minimize the fuel consumption. Assuming $\mathbf{x} = [t_{\text{ToF}}, T_0, \eta_0]^T$, the cost function is $f(\mathbf{x}) = m(t_0) - m(t_{\text{f}})$, and the problem can be expressed in the form:

$$\min_{\mathbf{x}} f(\mathbf{x}) \text{ such that } \begin{cases} \mathbf{x}_L \leq \mathbf{x} \leq \mathbf{x}_U \\ \mathbf{c}_L \leq \mathbf{c}(\mathbf{x}) \leq \mathbf{c}_U \end{cases} . \tag{28}$$

The optimization variables $\mathbf{x}$ are not allowed to assume any value, but they have a finite domain with lower bound $\mathbf{x}_L$ and upper bound $\mathbf{x}_U$. These are called *box constraints*.

The time-of-flight must be greater than zero, but is not possible to determine an upper bound with a proper physical meaning. In fact, during a landing maneuver, the thrust could assume null or negligible values for long (potentially indefinite) times. Actually, the presence of a gravity field limits the optimum t_{tof} to reasonable values:

$$0 \leq t_{\text{tof}} \leq \sqrt{\frac{2r_0^2 h_0}{\mu}}, \tag{29}$$

where h_0 is the initial altitude over the asteroid, and μ is its gravitational parameter:

$$\mu = G\rho \frac{4\pi}{3} abc, \tag{30}$$

where G is the universal gravitational constant, a, b, c semi-axes of the ellipsoid. The adopted upper bound represents the time that the spacecraft would take to cover a distance equal to h_0 in free fall, if subject to a constant acceleration of gravity equal to $\mathbf{g}(\mathbf{r}_0)$. It has no real physical meaning, but it has the proper order of magnitude (2-3 times the optimal t_{tof}) for an efficient optimum search.

The thrust magnitude is bounded to the thrust available on-board:

$$-T_{\text{max}} \leq T_0 \leq T_{\text{max}}. \tag{31}$$

The initial thrust angle bounds should be large enough to cover every direction in the plane:

$$-\frac{\pi}{2} \leq \eta_0 \leq \frac{\pi}{2}. \tag{32}$$

The elements of $\mathbf{c}(\mathbf{x})$ are generally non-linear functions of the optimization variables, also bounded between lower and upper limits $\mathbf{c}_L$ and $\mathbf{c}_U$. These constraints need to be satisfied during all the landing maneuver, so they are called *path constraints*.

During the landing the required thrust magnitude cannot exceed the limit imposed by the actual engine on board. Since the control action is evaluated in terms of acceleration, the corresponding thrust should depends on the actual spacecraft mass, according to the Newton's second law. Actually, the relatively small fuel consumption in low gravity environments allows to consider the mass as constant in the constraints evaluation:

$$0 \leq \|\mathbf{a}_{\text{c}}(t)\| \leq \frac{T_{\text{max}}}{m_0}. \tag{33}$$

Along a feasible landing path the altitude is always greater than zero. This constraint can be improved considering a *glide-slope constraint*. In this case the spacecraft is required to remain in a cone, pointing at the target landing site and defined by the maximum slope angle $\delta_{\max}$, as showed in Figure 3. This constraint has a dual purpose: it assures that the the spacecraft does not penetrate the

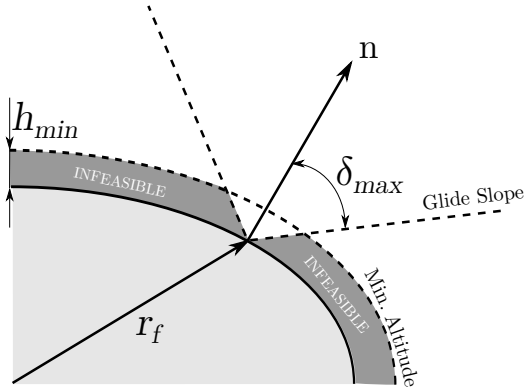

Figure 3. Glide-slope and minimum altitude constraints.

ground, even in presence of bulky terrain features near the landing site, while limiting at the same time the angle of view onto the target. In fact, the performances of vision-based navigation systems depend on inclination between the trajectory and the ground.[13,14]

Due to the small dimension of the target, it is possible that the maneuver starts from a position that does not satisfy this constraint. In this case is required that the spacecraft remains over a minimum altitude as long as it doesn't enter the cone. The j-th general constraint on trajectory shape can be represented in the form:

$$-\infty \leq \|\mathrm{S}_j\mathbf{r}(t) - \mathbf{b}_j\| + \mathbf{c}_j^T\mathbf{r}(t) + a_j \leq 0, \tag{34}$$

where $\mathrm{S}_j \in \mathbb{R}^{3\times3}$, $\mathbf{b}_j \in \mathbb{R}^3$, $\mathbf{c}_j \in \mathbb{R}^3$ and $a_j \in \mathbb{R}$. In the case of the glide-slope cone, we have:

$$\mathrm{S_g} = \mathrm{I} - \mathbf{n}\mathbf{n}^T, \tag{35}$$

$$\mathbf{b_g} = \mathrm{S_g}\mathbf{r_f}, \tag{36}$$

$$\mathbf{c}_\mathrm{g}^T = -\tan(\delta_{\max})\mathbf{n}^T, \tag{37}$$

$$a_\mathrm{g} = -\mathbf{c}_\mathrm{g}^T\mathbf{r}_\mathrm{f}, \tag{38}$$

where $\mathbf{n}$ is the unit vector normal to the ground at the target landing site. The constraint on minimum altitude $h_{\min}$ for a tri-axial ellipsoid can be expressed with:

$$\mathrm{S_h} = -\operatorname{diag}\big([\beta\gamma, \alpha\gamma, \alpha\beta]\big), \tag{39}$$

$$\mathbf{b}_\mathrm{h} = 0, \tag{40}$$

$$\mathbf{c}_\mathrm{h}^T = 0, \tag{41}$$

$$a_\mathrm{h} = -\alpha\beta\gamma, \tag{42}$$

where $\alpha = a + h_{\text{min}}$, $\beta = b + h_{\text{min}}$ and $\gamma = c + h_{\text{min}}$. Glide-slope cone and minimum altitude can be bounded in a single trajectory constraint through the inequality:

$$-\infty \leq \min(C_g, C_h) \leq 0, \tag{43}$$

where:

$$C_{\text{g}} = \|\text{S}_{\text{g}}\mathbf{r}(t) - \mathbf{b}_{\text{g}}\| + \mathbf{c}_{\text{g}}^T\mathbf{r}(t) + a_{\text{g}}, \tag{44}$$

$$C_{\text{h}} = \|\text{S}_{\text{h}}\mathbf{r}(t)\| + a_{\text{g}}. \tag{45}$$

Path constraints need to be satisfied at every time instant during the landing. Pseudospectral techniques allow to evaluate them discretely at Chebyshev-Gauss-Lobatto points.

Finally, the polynomial formulation does not explicitly consider boundary constraints on mass. This implies the additional constraint:

$$m_{\text{dry}} \leq m(t_{\text{f}}) \leq m_0. \tag{46}$$

OPTIMIZATION ALGORITHM

The optimization problem (28) can be solved through many different algorithms. In this case, fast computation must be privileged, in perspective of a real-time implementation for on-board hardware. In this context, direct optimization methods are attractive, because they don't require any derivation of necessary conditions, treating the cost function as a "black-box".[4,5]

In this work, a modified version of the *compass search method*, enhanced in order to handle also non-linear constraints, is adopted. In this paper, only the modifications applied for non-linear constraints are described. For a detailed description of the classical compass search method, see Reference 15.

First, the optimization variables are normalized, in order to give them the same relative weight in the optimization:

$$\tilde{\mathbf{x}} = \frac{\mathbf{x} - \mathbf{x}_L}{\mathbf{x}_U - \mathbf{x}_L} \quad \Leftrightarrow \quad \mathbf{x} = \tilde{\mathbf{x}}(\mathbf{x}_U - \mathbf{x}_L) + \mathbf{x}_L. \tag{47}$$

Normalized optimization variables can vary between 0 and 1. Then, a feasibility function $F(\tilde{\mathbf{x}})$ is created, defined as:

$$F(\tilde{\mathbf{x}}) = \sum_{j=0}^{N_C} \frac{1}{w_{\text{F}j}} \max(0, \tilde{c}_j), \tag{48}$$

where $\tilde{c}_j$ are the components of a generalized constraints vector $\tilde{\mathbf{c}}(\tilde{\mathbf{x}})$, and $\mathbf{w}_{\text{F}}$ is a vector of weights, in order to normalize different constraints that can have different orders of magnitude:

$$\tilde{\mathbf{c}}(\tilde{\mathbf{x}}) = \begin{bmatrix} \mathbf{c}_L - \mathbf{c}(\tilde{\mathbf{x}}) \\ \mathbf{c}(\tilde{\mathbf{x}}) - \mathbf{c}_U \\ 0 - \tilde{\mathbf{x}} \\ \tilde{\mathbf{x}} - 1 \end{bmatrix}, \quad \mathbf{w}_{\text{F}} = \begin{bmatrix} \mathbf{c}_U - \mathbf{c}_L \\ \mathbf{c}_U - \mathbf{c}_L \\ \mathbf{x}_U - \mathbf{x}_L \\ \mathbf{x}_U - \mathbf{x}_L \end{bmatrix}. \tag{49}$$

The trajectory constraint lower bound (43), and consequently the corresponding weight, is infinite. In order to avoid an improper constraint evaluation, this weight is set to h_{min}, that have the correct order of magnitude.

A feasible set of optimization variables $\tilde{\mathbf{x}}$ corresponds to a null value of the feasibility function. On the contrary, in case of infeasibility, $F(\tilde{\mathbf{x}}) > 0$.

The optimization algorithm operates in two phases. Firstly, an unconstrained compass search on the function $F(\tilde{\mathbf{x}})$ is performed. The search is stopped when a feasible point is found ($F(\tilde{\mathbf{x}}) = 0$), or when the iteration limit is reached. In this case, the problem is classified as infeasible.

If the fist step is successful the algorithm keeps solving for the optimum through an unconstrained search on the modified cost function $\Phi(\tilde{\mathbf{x}})$, defined as:

$$\Phi(\tilde{\mathbf{x}}) = f(\tilde{\mathbf{x}}) + \xi \operatorname{sgn}\big(F(\tilde{\mathbf{x}})\big), \tag{50}$$

where $f(\tilde{\mathbf{x}})$ is the original cost function of the problem (28), and $\xi = 10^{100}$, a number certainly greater than the maximum value that cost function can assume.

ALGORITHM VALIDATION AND TEST

The guidance algorithm have been tested through a Monte Carlo test campaign, implemented in MATLAB® and Simulink® environment, in series of 300 shots, reproducing a plausible scenario of asteroid landing. As representative target, the asteroid 1999 RQ_{36} "Bennu" (objective of the next NEA mission, OSIRIS-REx, planned for launch by NASA in 2017)[9] has been selected (see Table 1 for considered asteroid nominal parameters).

In this paper, an example of an equatorial landing is presented. The spacecraft is supposed to start at a near hovering condition. The target state is on the vertical over the selected landing site, at 3 m of altitude, with a vertical speed of $0.1\,\mathrm{m\,s^{-1}}$ toward the ground and a null horizontal speed. Spacecraft nominal initial and final states are summarized in Table 2. The adopted parameters dispersion, common to all the simulation here presented, is shown in Table 3.

Table 1. 1999 RQ_{36} "Bennu" nominal parameters.

Feature	Value	UoM
Major semi-axis, a	350	m
Intermediate semi-axis, b	287	m
Minor semi-axis, c	250	m
Density, ρ	1400	$\mathrm{kg\,m^{-3}}$
Rotational rate, ω	4.04×10^{-4}	$\mathrm{rad\,s^{-1}}$

Table 2. Spacecraft nominal parameters, initial and target states.

Feature	Value	UoM
Initial Position, $\mathbf{r}_0$	$[1500, 0, 0]^T$	m
Initial Velocity, $\mathbf{v}_0$	$[0, 0, 0]^T$	$\mathrm{m\,s^{-1}}$
Initial Mass, m_0	750	kg
Final Position, $\mathbf{r}_\mathrm{f}$	$[0, 290, 0]^T$	m
Final Velocity, $\mathbf{v}_\mathrm{f}$	$[0, -0.1, 0]^T$	$\mathrm{m\,s^{-1}}$
Specific Impulse, I_sp	315	s
Max Available Thrust, T_max	10	N
Dry Mass, m_dry	740	kg

Table 3. Monte Carlo parameters dispersion.

Parameter	Nominal Value	1σ
Initial Position, $\mathbf{r}_0$	$[1500, 0, 0]^T$ m	$\pm[50, 100, 100]^T$ m
Initial Velocity, $\mathbf{v}_0$	$[0, 0, 0]^T$ m s^{-1}	$\pm[0.1, 0.1, 0.1]^T$ m s^{-1}
Asteroid Density, ρ	1400 kg m^{-3}	$\pm 10\%$
Asteroid Rotational rate, ω	4.04×10^{-4} rad s^{-1}	$\pm 10\%$

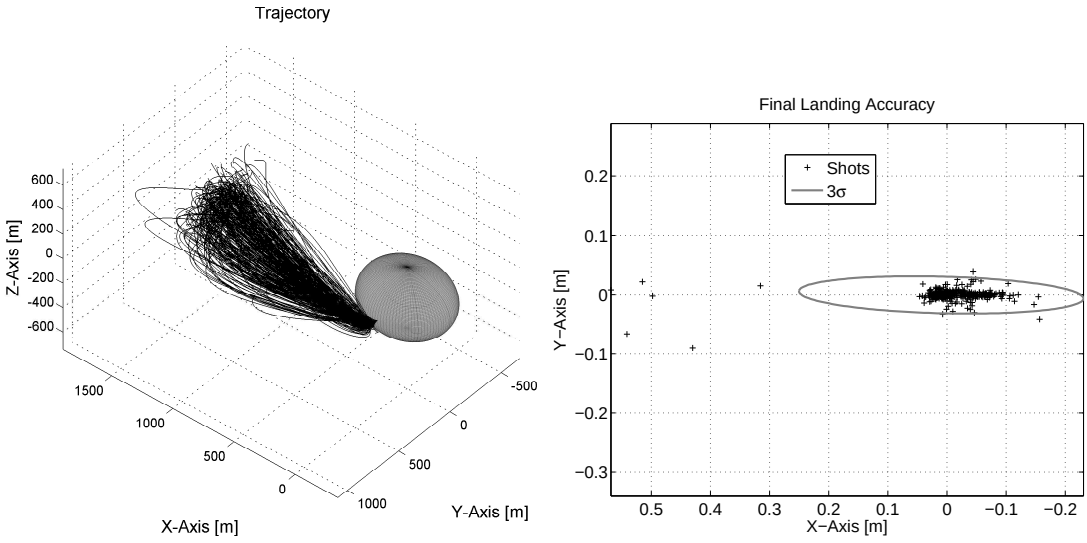

Figure 4. Theoretical guidance simulation. Left: 3D trajectories. Right: attained position at landing, with 3σ precision ellipse.

Theoretical Performance

In the first series of simulations, the system of equations (5)-(11) has been implemented as is, in order to assess the theoretical precision of the algorithm. The thrust obtained from the polynomial acceleration profile computed during the optimization process has been directly applied to the dynamic system.

In Figure 4 the trajectories and the precision obtained at landing are shown. The algorithm is theoretically able to find feasible paths to the target. Figure 5 shows how also the other states converge to the target with minimal error.

Thrust Modulation Effect

The optimized thrust profile describes essentially a low-thrust maneuver. The theoretical trust can assume very low values (also for long times) that could be not attainable by traditional propulsion systems. Then, it has been assumed that the thrust is supplied by the same system of chemical thrusters used by ACS, filtered by a Pulse-Width, Pulse-Frequency (PWPF) modulation system.

Sharing of the propulsion system is made possible by the slow dynamics of both attitude and thrust control systems. During the landing maneuver, the spacecraft must simply point toward the asteroid center of mass. the actual system architecture is represented in Figure 6. This configuration presents several advantages:

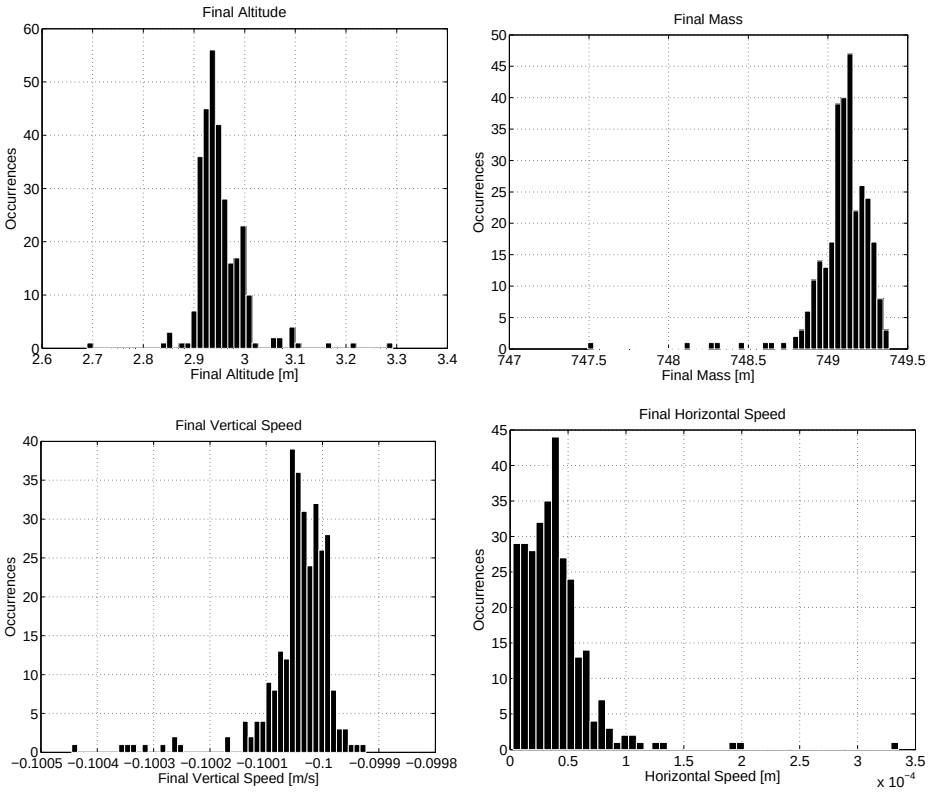

Figure 5. Theoretical guidance simulation, states dispersion at landing. Top-left: final altitude; Top-right: final mass; Bottom-left: final vertical velocity; Bottom-right: final horizontal speed (absolute value).

- The 3 components of the thrust vector can be generated independently, in body axes, leaving the spacecraft free to assume any attitude imposed by vision-based navigation system.

- There is no need of additional dedicated devices devoted to low-thrust.

- No additional constraints are imposed over high-trust propulsion system (devoted to high scale orbital control), in terms of thrust throttleability or minimum thrust level.

Then, a second series of Monte Carlo simulations have been performed, in order to verify the effect of the thrust modulation on the guidance performance. A level of thrust of $\pm 10\,\mathrm{N}$ over each axis has been considered. In order to minimize dispersion due to the not perfect modulation, as the landing site gets closer the trajectory is updated; the calculation is performed at 1000, 500, 300, 200 and $150\,\mathrm{m}$ from the target.

Figures 8 and 7 show the system states trend during a landing maneuver. It can be seen that the modulation is able to correctly approximate the commanded thrust.

The obtained dispersion at landing is shown in Figures 9 and 10. Actually, the modulation of thrust introduces a certain error in the attained position over the landing site. Anyway this error remains into acceptable limits, with an obtained final maximum accuracy of $8\,\mathrm{m}$ (3σ) from the target.

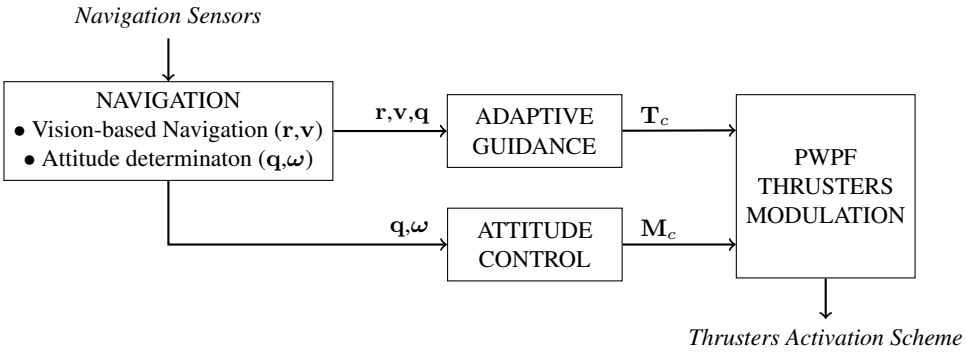

Figure 6. Logical schematic of the GNC System.

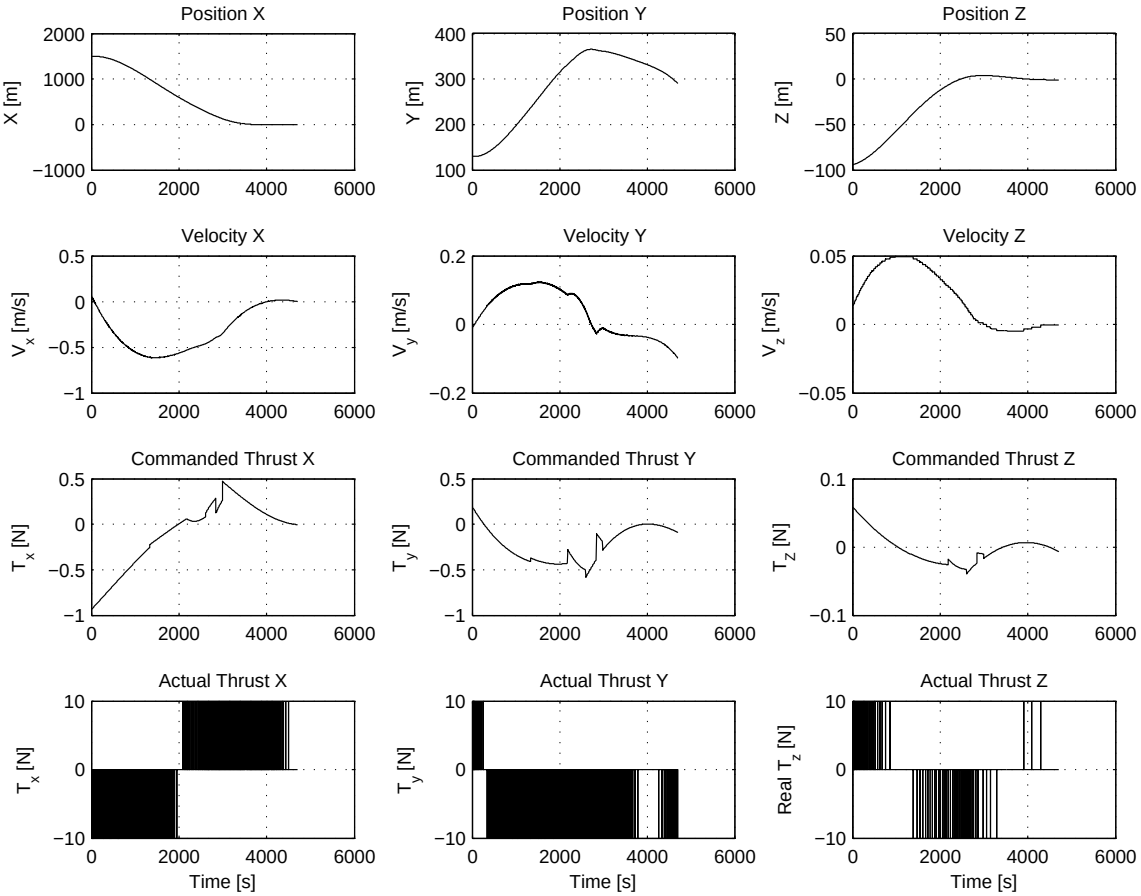

Figure 7. Example of landing maneuver with thrust modulaton.

Navigation Errors Effect

In the GNC schematic represented in Figure 6, is possible to see how navigation errors influence trajectory calculation. At the time the trajectory is recomputed, errors in position and velocity determination affects directly the obtained path. At the same time, since the thrust profile obtained

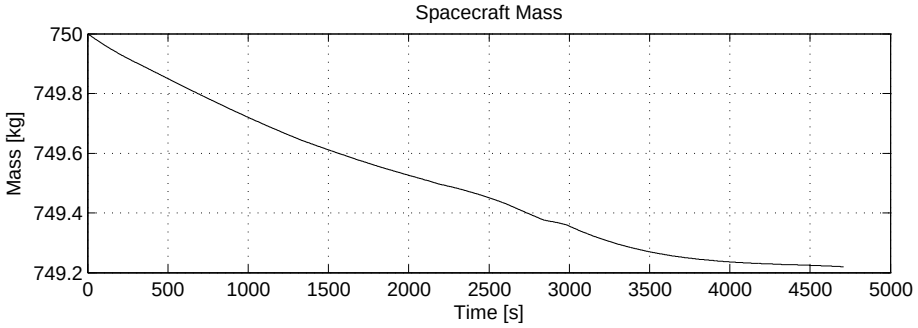

Figure 8. Example of landing maneuver with thrust modulaton, mass trend versus time.

from the optimization is expressed in asteroid reference frame, a conversion in spacecraft body-fixed frame is required at every control timestep in order to properly command the actuators. Then, errors in attitude determination affect the direction of the actual thrust, introducing additional errors in attained states at the maneuver's end.

For this reason, a third cycle of simulations has been performed, in order to verify the behavior of the system in presence of a real navigation system. Assuming the presence of a visual-based navigation system, errors in determination of position and velocity have been modeled as Gaussian errors, with zero mean and variable standard deviation proportional to the distance between the asteroid and the spacecraft. For attitude determination, the presence of a star tracker is assumed. All the considered error parameters are summarized in Table 4.

As in the previous case, the trajectory is updated as the spacecraft gets closer to the target, in order to limit dispersion at touchdown.

Obtained results are shown in Figures 11 and 12. Due to the relative long time requested by the maneuver, together with the applied open-loop control, errors in states determination at the retargeting epoch propagate up to potentially unacceptable values, especially for position (while a good precision in velocity is preserved).

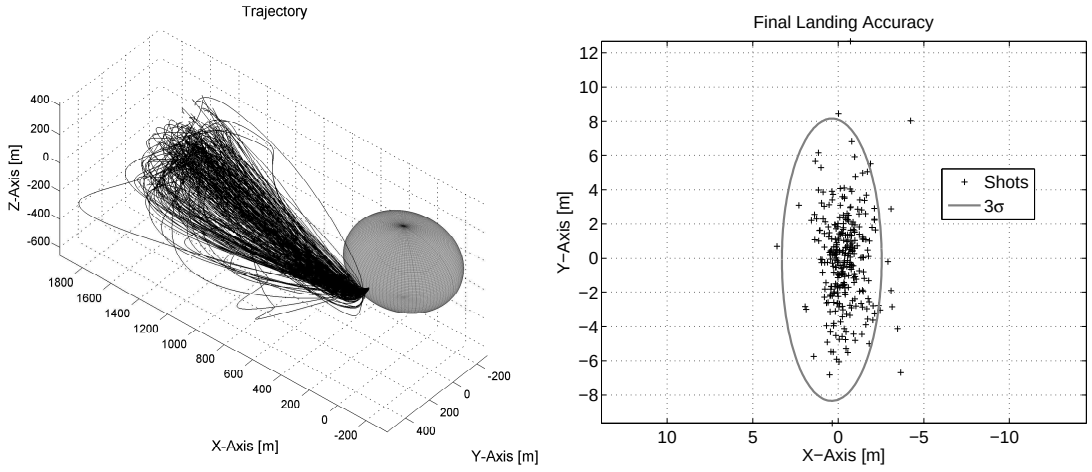

Figure 9. Landing simulation with modulated thrust. Left: 3D trajectories. Right: attained position at landing, with 3σ precision ellipse.

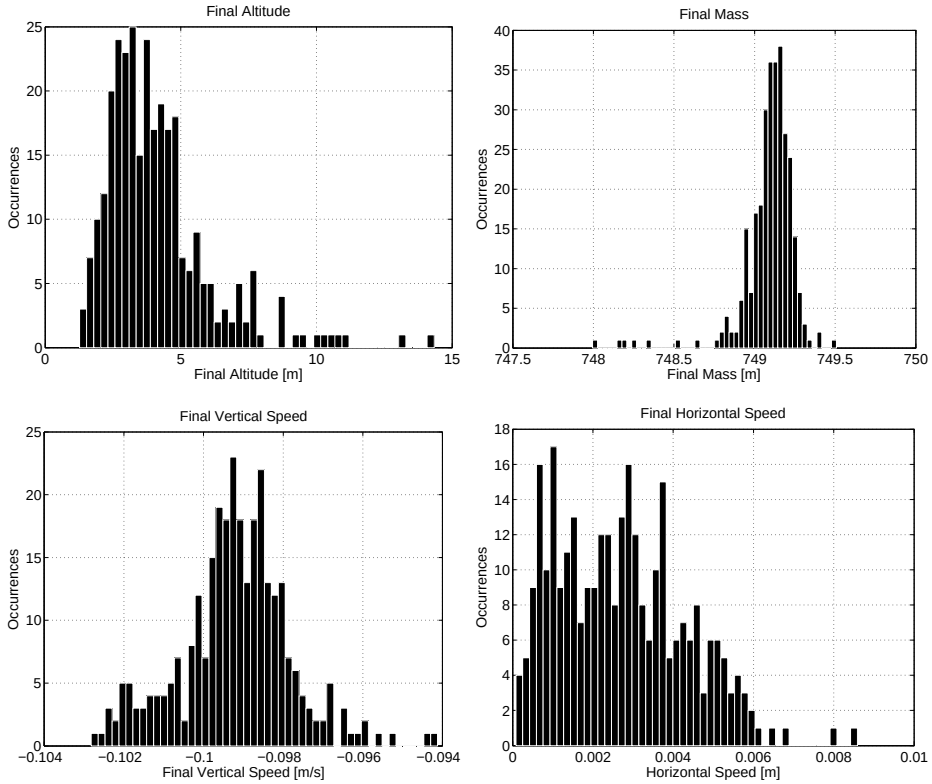

Figure 10. Landing simulation with modulated thrust, states dispersion at landing. Top-left: final altitude; Top-right: final mass; Bottom-left: final vertical velocity; Bottom-right: final horizontal speed (absolute value).

Table 4. Navigation errors parameters.

Parameter	**Nominal Value**	$\mathbf{1\sigma}$
Position error	$[0,0,0]^T$ m	$\pm[25,25,25]^T$ m @2000 m altitude
Velocity error	$[0,0,0]^T$ m s^{-1}	$\pm[0.1,0.1,0.1]^T$ m s^{-1} @2000 m altitude
Star tracker bias	5 arcsec	± 3 arcsec

A closed-loop approach, where the optimized trajectory is used as reference to be followed, should be able to drastically limit dispersion at touchdown, and is currently under investigation.

CONCLUSIONS

The purpose of this work was the development of a retargeting algorithm for landing maneuvers on low gravity non cooperative objects, capable of updating and correcting a landing trajectory almost to the touchdown.

A classical polynomial approach has been extended, in order to improve flexibility in the landing site choice, and to consider additional non linear constraints during the descent. The resulting algorithm has light computational weight, and maintains a high divert capability even with the use of a basic optimization algorithm such as compass search.

The functionality and the robustness of the algorithm have been tested by applying it in a Monte

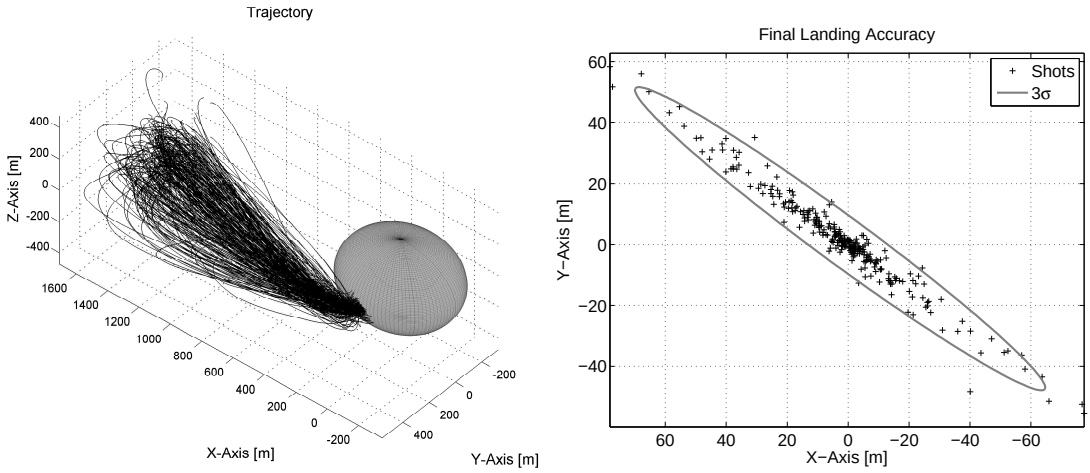

Figure 11. Landing simulation with modulated thrust and navigation errors. Left: 3D trajectories. Right: attained position at landing, with 3σ precision ellipse.

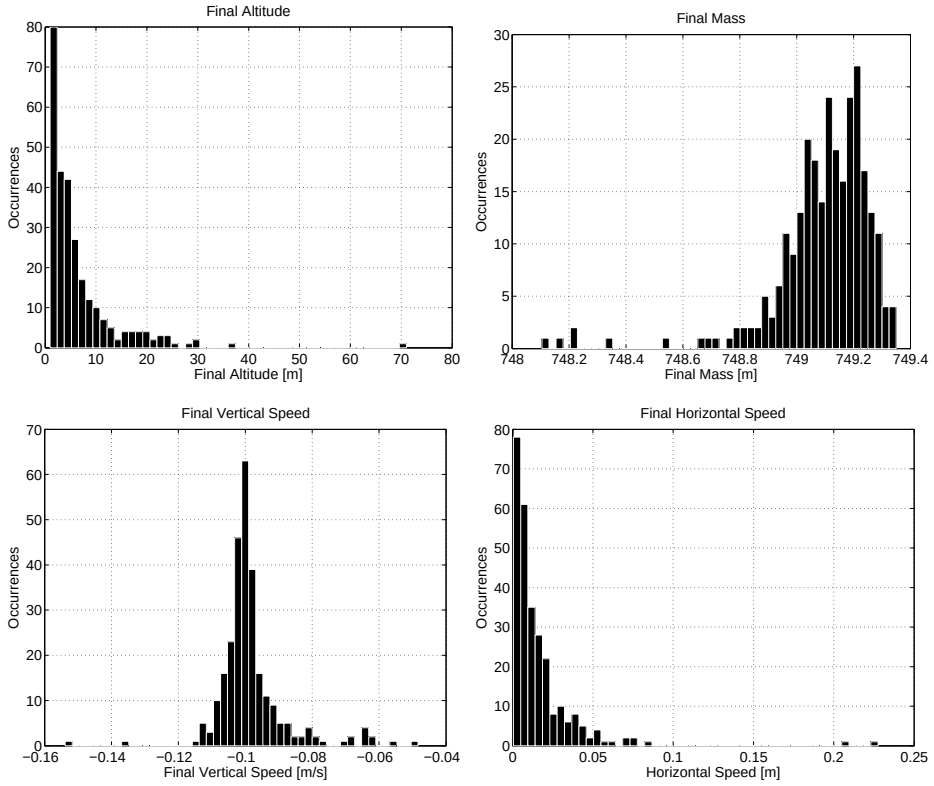

Figure 12. Landing simulation with modulated thrust and navigation errors, states dispersion at landing. Top-left: final altitude; Top-right: final mass; Bottom-left: final vertical velocity; Bottom-right: final horizontal speed (absolute value).

Carlo test campaign. Landing dispersion induced by the modulation of thrust and by navigation errors in open-loop control have been investigated.

It has been observed that while thrust modulation introduces a relatively small error, navigation

errors play a major role in determining the accuracy at touchdown. Due to the large duration of the maneuver, errors in position and velocity at the retargeting epoch can propagate up to potentially unacceptable values.

A closed-loop control approach, that considers the optimized trajectory as reference to be followed, should be able to avoid this error propagation, and is currently under investigation.

REFERENCES

[1] A. R. Klumpp, "Apollo lunar descent guidance," *Automatica*, Vol. 10, No. 2, 1974, pp. 133–146.

[2] E. Wong, J. Masciarelli, and G. Singh, "Autonomous Guidance and Control Design for Hazard Avoidance and Safe Landing on Mars," *AIAA Atmospheric Flight Mechanics Conference and Exhibit*, American Institute of Aeronautics and Astronautics, 2002.

[3] J. T. Betts, "Survey of Numerical Methods for Trajectory Optimization," *Journal of Guidance, Control, and Dynamics*, Vol. 21, No. 2, 1998, pp. 193–207.

[4] F. Fahroo and I. M. Ross, "Direct trajectory optimization by a Chebyshev pseudospectral method," *Journal of Guidance, Control and Dynamics*, Vol. 25, No. 1, 2002.

[5] B. Acikmeşe and S. R. Ploen, "Convex Programming Approach to Powered Descent Guidance for Mars Landing," *Journal of Guidance, Control and Dynamics*, Vol. 30, No. 5, 2007.

[6] M. Lara and D. Scheeres, "Stability bounds for three-dimensional motion close to asteroids," *Journal of the Astronautical Sciences*, Vol. 50, No. 4, 2003, pp. 389–409.

[7] M. Hawkins, Y. Guo, and B. Wie, "ZEM/ZEV Feedback Guidance Application to Fuel-Efficient Orbital Maneuvers Around an Irregular-Shaped Asteroid," *AIAA Guidance, Navigation, and Control Conference*, American Institute of Aeronautics and Astronautics, Aug 2012.

[8] R. Furfaro, D. Cersosimo, and D. Wibben, "Asteroid precision landing via multiple sliding surfaces guidance techniques," *Journal of Guidance, Control, and Dynamics*, Vol. 36, No. 4, 2013, pp. 1075–1092.

[9] R. Furfaro, B. Gaudet, D. Wibben, and J. Simo, "Development of non-linear guidance algorithms for asteroids close-proximity operations," *AIAA Guidance, Navigation, and Control (GNC) Conference*, American Institute of Aeronautics and Astronautics, 2013.

[10] P. Lunghi, M. Lavagna, and R. Armellin, "Adaptive Semi-Analytical Guidance for Autonomous Planetary Landing," *64th International Astronautical Congress - IAC 2013*, Beijing, China, International Astronautical Federation, Sept 2013.

[11] D. J. Scheeres, "Dynamics about Uniformly Rotating Triaxial Ellipsoids: Applications to Asteroids," *Icarus*, Vol. 110, No. 2, 1994, pp. 225–238.

[12] L. N. Trefethen, *Spectral methods in Matlab*. Society for Industrial and Applied Mathematics, 2000.

[13] G. Flandin, B. Polle, N. Despré, J. Lheritier, N. Perrimon, and P. Blanc-Paques, "Maturing Vision Based Navigation Solutions to Space Exploration," *AIAA Guidance, Navigation, and Control Conference*, American Institute of Aeronautics and Astronautics, 2010.

[14] J. Riedel, A. Vaughan, R. A. Werner, W. Tseng-Chan, S. Nolet, D. Myers, N. Mastrodemos, A. Lee, C. Grasso, T. Ely, and D. Bayard, "Optical Navigation Plan and Strategy for the Lunar Lander Altair; OpNav for Lunar and other Crewed and Robotic Exploration Applications," *AIAA Guidance, Navigation, and Control Conference*, American Institute of Aeronautics and Astronautics, 2010.

[15] T. Kolda, R. Lewis, and V. Torczon, "Optimization by Direct Search: New Perspectives on Some Classical and Modern Methods," *SIAM Review*, Vol. 45, No. 3, 2003, pp. 385–482.